

Numerical Simulation and Experimental Study on a New Type of Variable-rate Fluidic Sprinkler

J. P. Liu^{1*}, S. Q. Yuan¹, H. Li¹, and X. Y. Zhu¹

ABSTRACT

Due to the complex structure of the pressure-adjusting device used in most sprinklers for variable irrigation, it is not possible to observe the flow behavior of the water passing through the flow field. In this paper, an integral three dimensional (3D) numerical model based on the structural characteristics of the fluidic sprinkler was constructed to simulate the flow field distribution using computational fluid dynamics (CFD). A new type of fluid sprinkler (BPXH) was used in the experiments. The main stream region and the variable velocity regions were clearly distinguished, and the details of the variations in pressure are discussed. The results indicated that the simulation methodology generated sufficient data to analyze the sprinkler pressure and outlet velocity changes. The minimum error of the difference between the simulation and the test pressure values was 0.049, with a maximum of 0.14. The turbulence model could accurately predict the relationship between the outlet velocity and the wetted radius. The outlet velocity ranged from 12.6 to 17.9 m s⁻¹ during the simulation under the variable inlet boundary conditions of the sprinkler. Both the simulation and test values of the wetted radius increased gradually with the sprinkler rotating angle. The absolute error of the simulation and the test ranged from 0.07 to 0.16. Computational fluid dynamics provides a promising tool to help in the design of pressure-adjusting devices using a new type of variable-rate fluidic sprinkler.

Keywords: Fluidic sprinkler, Inner flow field, Numerical simulation.

INTRODUCTION

As water supplies become limited, agricultural water use needs to become more efficient to increase water productivity levels. Tso (2004) pointed out that the three most important resources -people, land, and water- must be effectively used to improve agricultural productivity and take advantage of new initiatives. With the rapid development of water-saving agriculture (Ahmadi *et al.*, 2009), sprinkler irrigation has been widely applied due to its high efficiency and economics (Keller and Bliesner, 1990).

Sprinkler is the key component in a sprinkler irrigation system. The performance of the sprinkler directly affects crop yield

and water losses. Most studies about sprinkler irrigation have focused on hydraulic performance (Sourell *et al.*, 2003; Hendawi *et al.*, 2005). An analysis of the flow behavior of the water flow in the sprinkler inner field is also important to understand the micro-characteristics of the sprinkler. Researchers have used numerical simulation to solve water flow modeling problems. Wang (2006) analyzed the flow characteristics in the emitter used in drip irrigation inner field using computational fluid dynamics (CFD) techniques and adopted the problem-solving methods used in CFD techniques to irrigation equipment. It can simulate the flow behaviors using CFD to obtain pressure and velocity distribution results (Anderson, 2004). Some

¹ Research Center of Fluid Machinery Engineering and Technology, Jiangsu University, 301 Xuefu Road, Zhenjiang, Jiangsu, People's Republic of China.

* Corresponding author; e-mail: liujunping401@163.com



basic studies have been performed on the inner flow characteristics of sprinklers. In 1933, the designer at the company Rainbird (Li *et al.*, 1995) developed an impact sprinkler for the first time. Experiments were performed to evaluate the inner flow characteristics of the impact sprinkler compartment, and pressure losses were analyzed using ANSYS software (Yan and Jin, 2004; Yan *et al.*, 2007). Yan *et al.* (2009) performed a 3D turbulent simulation to analyze the flow behavior in an impact sprinkler using CFD techniques and compared the flow rate, static pressure distribution and kinetic energy values of different current stabilizers. In 2005, researchers at Jiangsu University in China developed a new type of fluidic sprinkler. The new sprinkler is shown in Figure 1.

The pressure difference can be modeled discretely as arising from the signal tube, and the direction of the flow can be modified, which provides the force to run the sprinkler. Compared to the sprinklers studied previously, the structure of the new fluidic sprinkler is simpler, and the hydraulic performance is excellent (Li *et al.*, 2010). Studies of the new fluidic sprinkler have focused on the nozzle. In these studies, the inner flow field of the nozzle was simulated, and the pressure distribution was obtained (Yuan *et al.*, 2005; Li *et al.*, 2004).

However, on the basis of these successful studies, few other investigations have been conducted on the full flow field, and studies on complete simulations of the sprinkler

have been limited. The micro-characteristics of the sprinkler remain to be evaluated. With the development of Low Energy Precision Application (LEPA), the working pressure can be changed while the sprinkler is running (Fraisie *et al.*, 1995; Perry *et al.*, 2004). Implementing LEPA with the new fluidic sprinkler involves the addition of a pressure-adjusting device at the inlet that can change the working pressure while the sprinkler is running and also change the wetted radius. The structure of the new fluidic sprinkler (BPXH: Marked by the first letter of Chinese pronunciation) with the pressure adjusting device is shown in Figures 2 and 3.

The pressure adjusting device included swivel connection, connecting sleeve, static insert, movement insert, and hollow shaft. When the sprinkler is operating, the inlet section area can be changed, thus, changing the working pressure and the wetted radius. As can be seen in Figures 2 and 3, in the variable-rate fluidic sprinkler, one of the moving inserts is stationary and is referred to as the static insert. The static insert is fixed on a swivel connection that does not rotate with the sprinkler. The movement insert is fitted on a hollow shaft that rotates with the sprinkler. The static insert and the movement insert move relative to each other to change the inlet section area, thus, changing the working pressure of the sprinkler. Therefore, the wetted radius changes, and an irregularly shaped spray area can be covered.



(a) The new type of fluidic sprinkler



(b) Nozzle

Figure 1. The new type of fluidic sprinkler.

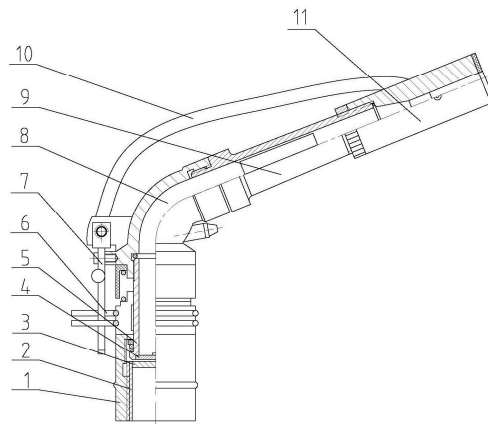


Figure 2. The structure of the new fluidic sprinkler with a pressure-adjusting device. (1) Swivel connection; (2) Connecting sleeve; (3) Static insert; (4) Movement insert; (5) Hollow shaft; (6) Location limit device; (7) Reversing device; (8) Spraying body; (9) Spraying pipe; (10) Plastic tube, (11) Nozzle.

Because of the pressure-adjusting device in the sprinkler, an irregular boundary spray area is obtained. As shown in Figure 4, the sprinklers are set at the location of O point. The R_0 is the wetted radius of a circle sprinkler, and R is the maximum wetted radius of the new fluidic sprinkler for square spray area. $R(t)$ is the wetted radius, which changes with time, and b is the minimum wetted radius of the new fluidic sprinkler. Therefore, when the sprinkler rotates for a round, the wetted square area with section lines is obtained.

The range and the adjusting device are important parameters of the performance. Therefore, the key compartment of the sprinkler needs to be studied using CFD techniques.

The objective of this study was to model the

structure of the new sprinkler features, to conduct a numerical simulation of the flow characteristics of the water field using the commercial CFD program FLUENT software, and to perform experiments to verify the simulation results.

MATERIALS AND METHODS

Numerical Simulation

Physical Model and Grid Generation

In this study, the BPXH20 fluidic sprinkler was chosen as the research object for a more

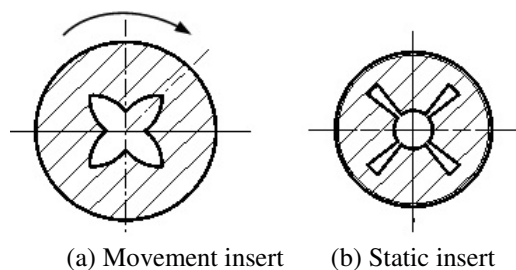


Figure 3. The structural chart of the moving inserts.

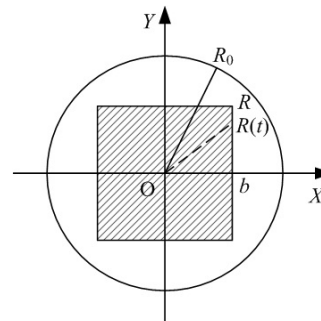


Figure 4. Schematic diagram of spraying shape



effective analysis. The physical model was the inner flow channel of the sprinkler.

Grid selection is an important technique to improve accuracy in the numerical simulation method. In this study, an unstructured mesh method was attempted as test/hybrid elements with grid type. Figure 5 shows a view of the grids of the physical model of the structure of the sprinkler used in the simulation. The entire model was meshed into 318,057 units. The mesh sensibility was tested using a smaller cell size, but no influence on the final results was found.

Mathematical Model

The inlet cross-section area was modified by two moving inserts in relative motion, the rotating velocity was $\omega = 0.06 \text{ rad s}^{-1}$, the material was water and the inlet pressure was higher than 0.2 MPa. The Reynolds number was calculated to be approximately 10^7 . The results showed that the flow field in the sprinkler was turbulent. Therefore, a turbulence model in FLUENT software was used to simulate the flow behavior under every operating condition to ensure a comprehensive analysis, and a steady flow unit was set in the flow channel.

There are some models in FLUENT

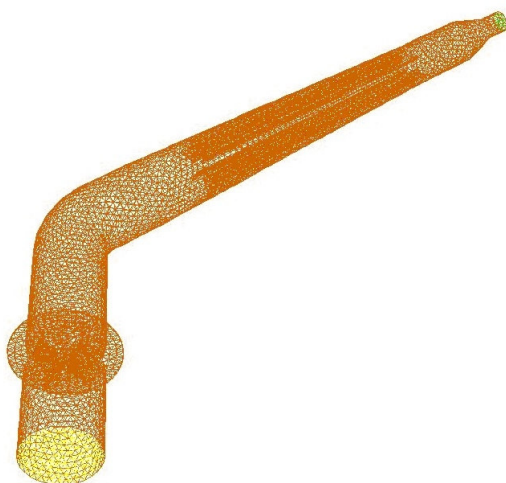


Figure 5. The computational grids of the numerical model.

software including standard $k - \epsilon$, RNG $k - \epsilon$, realizable $k - \epsilon$ and so on. Due to the smallest computational deviation error from the measured results, the standard $k - \epsilon$ model equations were chosen in this study. The standard $k - \epsilon$ turbulent model, which is generally used for most engineering calculations, was chosen to describe the flow in the sprinkler. The governing equations for the standard $k - \epsilon$ turbulent model in FLUENT software are given as follows (John, 2004):

Continuity equation:

$$\frac{\partial}{\partial x_i} (\rho u_i) = 0 \tag{1}$$

Navier-Stokes equation:

$$\frac{\partial}{\partial t} (\rho u_i) + \frac{\partial}{\partial x_i} (\rho u_i u_j) = -\frac{\partial p}{\partial x_i} + \frac{\partial}{\partial x_j} \left(\mu \frac{\partial u_i}{\partial x_j} \right) + S_i \tag{2}$$

k equation:

$$\frac{\partial(\rho k)}{\partial t} + \frac{\partial(\rho k u_i)}{\partial x_i} = \mu_t \left(\frac{\partial u_i}{\partial x_i} + \frac{\partial u_j}{\partial x_j} \right) \frac{\partial u_i}{\partial x_j} + \frac{\partial}{\partial x_j} \left[(\mu + \mu_t) \frac{\partial k}{\partial x_j} \right] - \rho \epsilon \tag{3}$$

ϵ equation:

$$\frac{\partial(\rho \epsilon)}{\partial t} + \frac{\partial(\rho \epsilon u_i)}{\partial x_i} = \frac{1}{2} \rho C_{\epsilon 1} \epsilon \left(\frac{\partial u_i}{\partial x_j} + \frac{\partial u_j}{\partial x_i} \right) + \frac{\partial}{\partial x_j} \left[(\mu + \mu_t / \sigma_\epsilon) \frac{\partial \epsilon}{\partial x_j} \right] - \rho C_{\epsilon 2} \frac{\epsilon^2}{k + \sqrt{v \epsilon}} \tag{4}$$

Where, k = Turbulent kinetic energy; ϵ = Rate of dissipation; ρ = Fluid density; u = Velocity of the flow at x component; x = Displacement vector; μ = Fluidic viscosity; p = Pressure; S_i = Source term; v = Velocity of the flow at y component; t = Time; i and j = Vectors, $C_{\epsilon 1}$, $C_{\epsilon 2}$ and σ_ϵ = Correcting coefficients.

Values of temperature during irrigation are not very large, hence, the flow in sprinkler are incompressible. These equations are used for calculating the moving fluid element of flow in the sprinkler. After calculation and solving Equations (1) to (4),

the velocity and pressure in the flow field can be obtained.

Boundary Conditions and the Numerical Method

Generally, sprinkle irrigation is implemented at a given pressure. This sprinkler works under variable pressure because of the pressure-adjusting device, that is, the inlet of the sprinkler does not keep a fixed pressure. The pressure and flow rate values at the different rotating angles of the sprinkler were adjusted. As shown in Figure 6, the movement insert and static insert were in the rotating angle of 0 to 45 degrees and the black part was the flow cross section. The movements insert rotated deasil and the angle increased. For square spraying shape, the varied flow cross section from 0° to 45° is the same with 45° to 90°, from 0° to 90° is the same with 90° to 180°, from 0° to 180° is the same with 180° to 360°. The flow can be calculated with rotation angle from 0° to 45°, and the values of other angles can be symmetrical. The flow rates were verified by test values. The velocity values were obtained from the flow value and the inlet section area. Next, the inlet boundary condition was set by the velocity, and the outlet boundary condition was set by the outflow. The inlet boundary conditions for the velocities used are shown in Table 1.

In near-wall treatment, three kinds of methods are available as Standard wall

Table 1. The inlet boundary conditions of the sprinkler.

Rotation angle (°)	0	15	30	45
Flow rate (m ³ h ⁻¹)	2.08	2.34	2.95	3.47
Velocity (m s ⁻¹)	1.84	2.07	2.37	2.61

functions, Non-equilibrium wall functions, and Enhanced wall treatment. With the advantages of less computation time and iteration steps, Standard wall functions were implemented. The continuity and Navier-Stokes equations were solved by using a SIMPLE Consistent (SIMPLEC) algorithm (embedded in FLUENT) proposed by Van Doormal and Raithby (1984). Compared to the impact of the water pressure, the effect of gravity was considered low and, therefore, the gravity of water was neglected. The convergence precision of the calculation was set at 0.0001.

Wetted Radius Calculation

We can also calculate the wetted radius by the formula developed by Tuo *et al.* (2006):

$$R = \frac{1}{K} \ln \left\{ 1 + KV_0 \cos \theta \left[\frac{1}{\sqrt{Kg}} + \arctan \sqrt{\frac{K}{g}} \right] V_0 \sin \theta \right. \\ \left. + \frac{h + \frac{1}{2} \left(\frac{1}{\sqrt{Kg}} + \arctan \sqrt{\frac{K}{g}} \right) (V_0 \sin \theta)}{\sqrt{\frac{g}{K}}} \right\} \quad (5)$$

Where, R = Wetted radius of the sprinkler (m); V_0 = (m s⁻¹); θ = Angle of the sprinkler

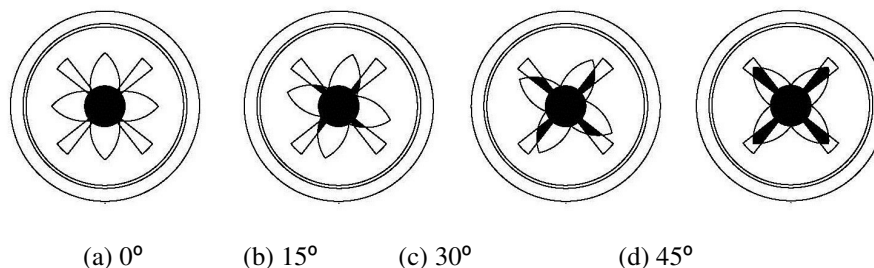


Figure 6. The flow cross section of the movement insert and static insert



(30°); g = Acceleration due to gravity (m s^{-2}), h = Installation height (1.2 m).

In Equation (5), the coefficient K is calculated as follows:

$$K = \frac{3}{4} \left(\frac{C_d}{d} \right) \left(\frac{\rho_a}{\rho_w} \right) \quad (6)$$

Where, C_d = The frictional resistance coefficient determined by the Reynolds number. In this paper, the Reynolds number is greater than 2320, and the value of the frictional resistance coefficient is 0.44. ρ_a = Air density (1.29 kg m^{-3}); d = Diameter of the sprinkler nozzle (8 mm), ρ_w = Water density ($1 \times 10^3 \text{ kg m}^{-3}$).

Therefore, the coefficient K can be calculated, and Equation (5) can be simplified as follows:

$$R = 18.79 \ln \{ 1 + 0.006V_0^2 + 0.00072V_0 \} \quad (7)$$

In Equation (7), when the V_0 value is obtained, the wetted radius can be calculated.

Experimental Procedure

The experimental platform was set up in the indoor laboratory of the Research Center of Fluid Machinery Engineering and Technology at Jiangsu University in China. There were no obstacles in the laboratory, and wind interference was eliminated. The experiments were conducted according to the standards of the American Society of Agricultural and Biological Engineers (ASABE) S436.1 and S398.1. The equipment for the experiment

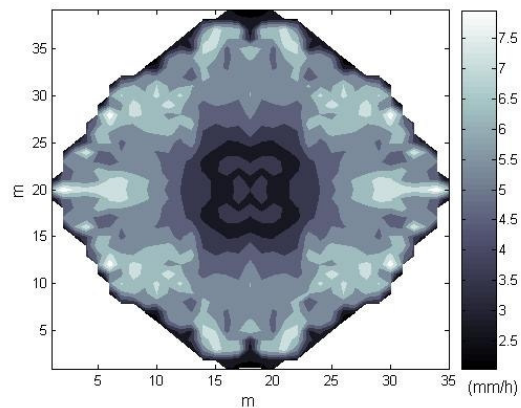


Figure 7. The wetted areas of square shape for the sprinkler.

included the fluidic sprinkler (model BPXH20, Shanghai Watex Water-economizer Technology Co, Ltd.), pipeline, pump system, and water collectors. The values of the pressure and flow rates for each sample were recorded, the experiment was performed three times, and the wetted radius was calculated ten times and then averaged.

The wetted area of square shape for the sprinkler is shown in Figure 7. The sprinkler was set in the center of the wetted area and, when the sprinkler rotated for a round, the pressure-adjusted device worked and produced a square wetted shape.

Although the wetted radius and uniformity experiments can be used to obtain the hydraulic performance of the sprinkler, they cannot be used to evaluate the small flow fields inside the channels. Consequently, an experiment was conducted using the test apparatus depicted schematically in Figure 8.

As shown in Figure 8, water was pumped

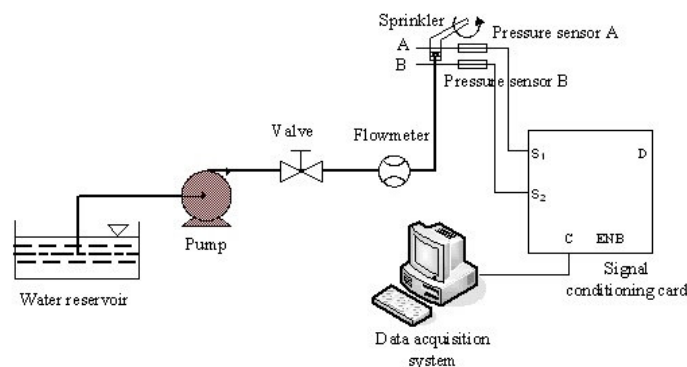


Figure 8. The schematic diagram of the experimental setup used to measure the flow fields of the sprinkler.

from the reservoir by a centrifugal pump (model IS80-50-250), and the volume of the water flowing through the sprinkler channels was measured using a flow meter (model MF/E5001621100EH11). To measure pressure difference between points A and B, pressure sensors A and B (model WT1151GP) were set at the points A and B, respectively. As shown in Figure 9, the flow characteristic through the pressure adjusting device and to the outlet, a distance of 50 mm, is stable. Impact of different distances (40, 50, 60, 70 mm) from the inlet were compared and little variations were found for the influence of pressure at 50, 60, and 70 mm distances. But, at the distance of 40 mm, the flow characteristic was unstable. Therefore, 50mm of point A from the inlet was chosen. The measurement range was 0 to 1 MPa, and the precision was $\pm 2\%$. When the sprinkler was rotated, the pressure sensors detected a change in the pressure value in the sprinkler inner flow field. The data acquisition and collection were performed using LabVIEW software ver. 8.2 (National Instrument Corp., Austin, Texas). The data sampling frequency rate was set at 1,000 Hz.

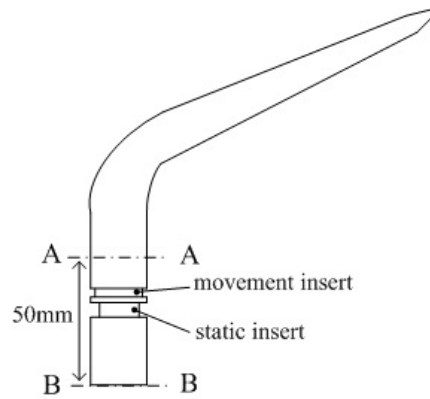


Figure 9. Schematic diagram of actual points A and B in the sprinkler.

rotation occurred at low pressure. The mainstream region and the variable velocity regions were clearly distinguished. The water flows through the pressure-adjusting device and the recirculation developed above the clearance can be seen in Figure 10. The flow pattern is turbulent. Figure 11 shows the velocity value in different distance from inlet cross section in different rotating angles. It can be seen in Figure 11 that the velocity value increased with increase in the rotating angle.

RESULTS AND DISCUSSION

Analysis of the Flow Characteristics

Figure 10 shows the velocity contours of the pressure-adjusting device and the velocity distribution when the sprinkler

Variation of Pressure

Figure 12 shows the pressure distribution of the sprinkler at different angles. The pressure increased as the angle of rotation of the sprinkler increased. The average pressure value at a 50 mm distance from the

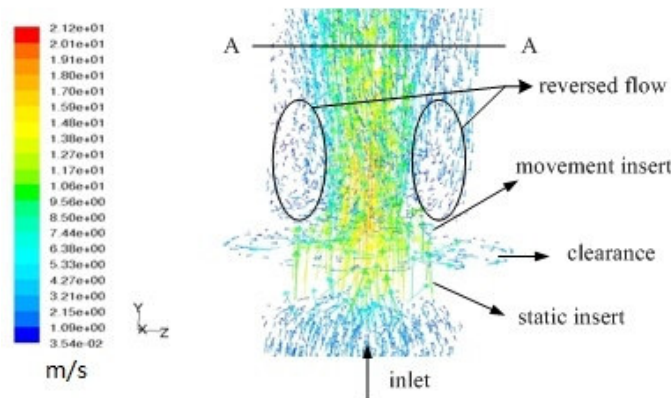


Figure 10. The contour of the velocity of the pressure-adjusting device at an angle of rotation.

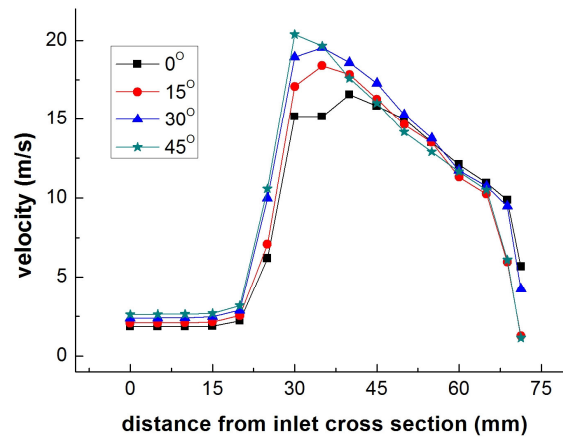


Figure 11. The velocity value in different distances from inlet cross section in different rotating angles.

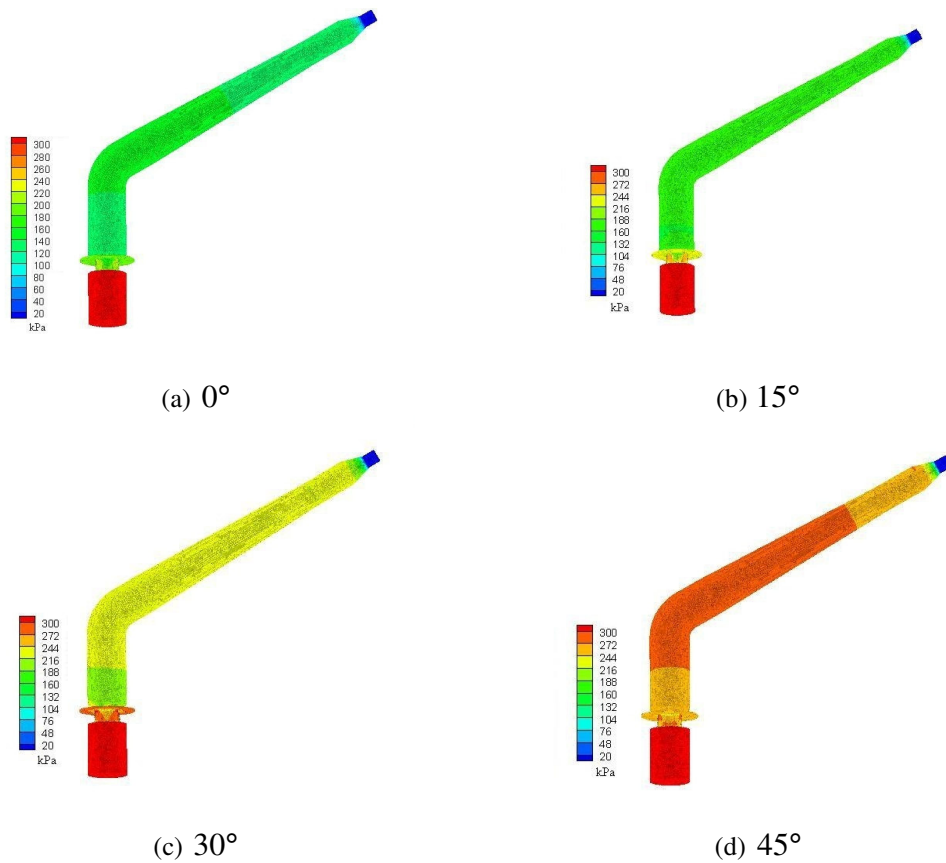


Figure 12. The pressure distribution of the sprinkler.

inlet is shown in Figure 13.

As shown in Figure 13, the pressure increased as the rotating angle increased and the minimum and maximum pressure values

were 0.128 and 0.265 MPa, respectively. At a distance of 50 mm from the inlet, the pressure changes with the rotating angle of the sprinkler. All statistical analyses were

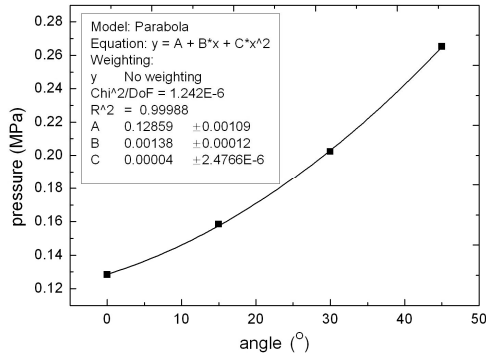


Figure 13. The pressure value at a 50 mm distance from the inlet of the sprinkler.

conducted using a 95% confidence interval. A second-order polynomial regression line ($y = 0.00004x^2 + 0.00138x + 0.12859$, where y is the pressure value at a location 50 mm from the sprinkler, x is the rotation angle of the sprinkler, and $r^2 = 0.99988$) was fitted to pressure and angle of rotation to estimate the difference between the test data and the simulation data.

Figure 14 shows the pressure values for sections A and B. In this diagram, P_B is the pressure at section B, the inlet of the sprinkler, and P_A is the pressure at section A, 50 mm from the inlet of the sprinkler. During the sprinkler rotation, pressure data were recorded for 28 seconds in this experiment. Figure 14 depicts the whole pressure drop from the inlet to the outlet over five periods. P_B is the working

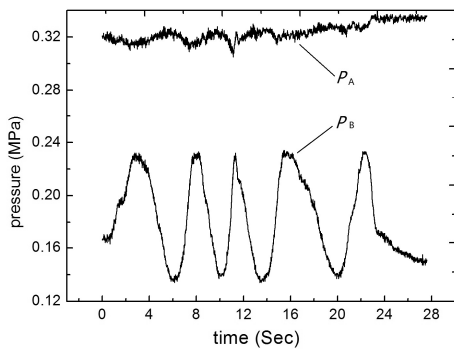


Figure 14. Pressure values for sections A and B.

pressure, and the range of P_B is larger than P_A . As shown in Figure 4, every quadrant is one period, and there are four quadrants for a complete round. The wetted radius for the square spraying area changed over four periods for a round when the sprinkler rotating and the inlet and outlet pressure also changed over those four periods. Therefore, we selected half of the periods over which the pressure fluctuated and transformed the pressure as a function of the angle of rotation instead of time. The simulation and test values were compared, and the results are presented in Figure 15.

As seen in Figure 15, the tendencies of the pressure P_A remained fairly constant. From 6.0 to 8.0 seconds, the pressure P_B increased. The minimum error of the difference between the simulation and the test pressure values was 0.049, while the maximum was 0.14. This indicated a very good agreement between simulation and test results. In contrast, the simulation values were larger than the experimental values during the period from 6.75 to 8.0 seconds. This is because the physical model is extremely clean, while, in reality, the sprinkler cannot be expected to be as clean; thus, during the sprinkler rotation, the axial clearance of the moving inserts may not be in good agreement with the physical model in the simulation. Therefore, the simulation results overestimated the pressure in the system.

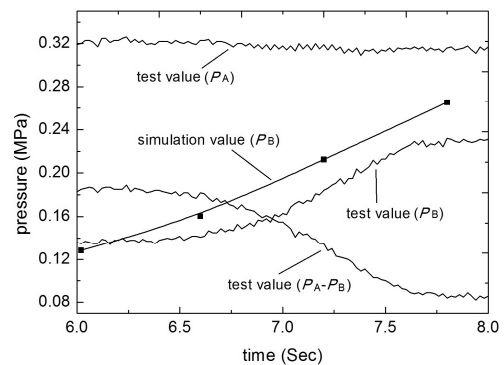


Figure 15. Comparison of the relationship between pressure and time from the simulation and the test.



Relationship of the Outlet Velocity and Wetted Radius

Theoretically, the outlet velocity plays an important role in determining the performance of the sprinkler wetted radius. The relationship between the outlet velocity and the wetted radius has to be determined to ensure the accuracy of the simulation model. When the sprinkler was rotating, the outlet velocity changed with the rotating angle. In this study, the lowest working pressure was found at the lowest section area and at an angle of zero degree. The sprinkler working pressure was changed in four periods, and a square shaped spraying area was obtained. The outlet velocity distributions of sprinkler nozzle areas are shown in Figure 16.

The sectional average velocity of the outlet at different angles was derived from the simulation, the outlet velocity ranged from 12.6 to 17.9 m s⁻¹ during the simulation

under the variable inlet boundary conditions of the sprinkler. The changed curve of the outlet velocity at different angles is presented in Figure 17, which shows that the outlet velocity increased gradually with the angle of rotation of the sprinkler. This occurs because the working pressure gradually increased with the sectional area of the sprinkler inlet. Therefore, the outlet velocity and the working pressure increased with the rotating angle.

The outlet velocity can be determined from the wetted radius. From the relationship between the outlet velocity and the wetted radius, the V_0 value in Equation (7) is derived by using the simulated velocity at the outlet. The relationship between the angle and the wetted radius obtained by simulation and experimentally, respectively, is shown in Figure 18. The values from simulation and experimentation were compared under the same conditions.

As seen in Figure 18, both the simulation

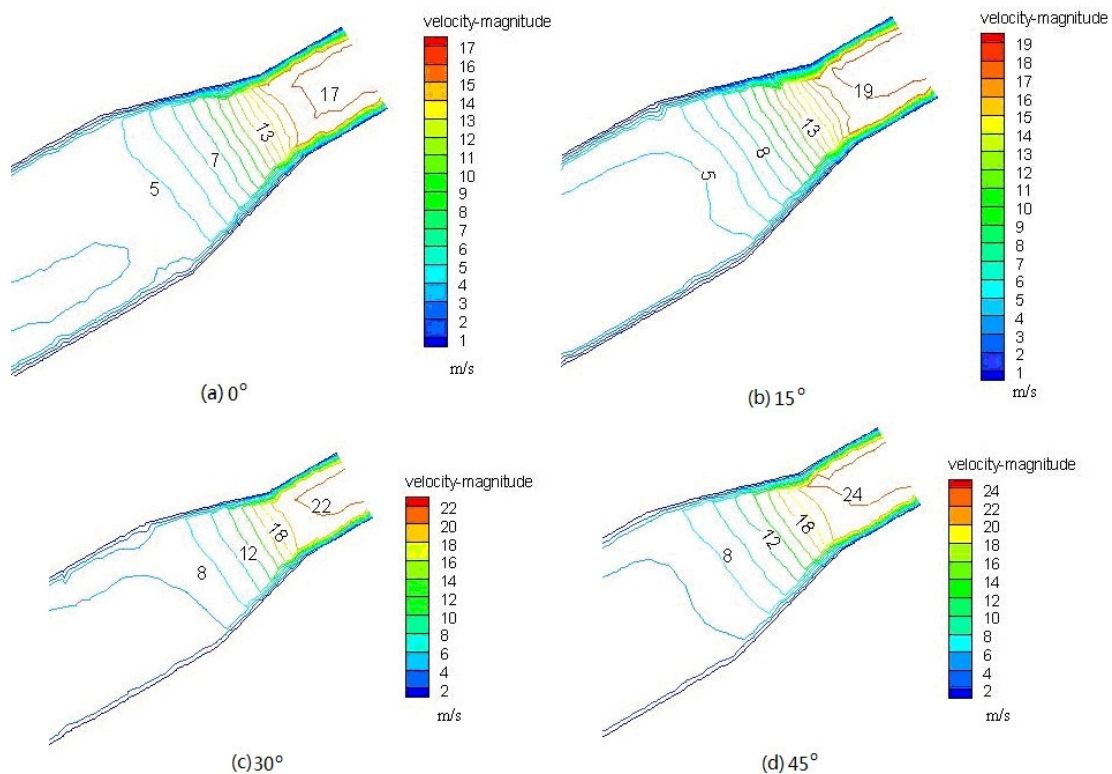


Figure 16. The outlet velocity distributions of sprinkler nozzle areas.

and test values of the wetted radius increase gradually with increase in the rotation angle of sprinkler and the two curves are almost parallel to each other; but, the test value is lower than the simulation value. The relative error of the simulation and test values ranged from 0.07 to 0.16. As well known, the bigger the pressure, the longer is the wetted radius. The reasons for the simulation values being larger than the test values of pressure apply to the wetted radius as well.

CONCLUSIONS

In this study, we conducted numerical simulations on the internal flow of the new fluidic sprinkler and performed experiments on the flow fields in the channels and on the hydraulic performance. We obtained the following results:

The turbulence model was applied in a simulation and the results indicated that the turbulence model can accurately predict the working pressure and the relationship between the outlet velocity and the wetted radius. By comparing the flow fields of the pressure-adjusting device, obtained by calculation and experiment, it is feasible to employ LabVIEW software to measure the flow characteristics. The variation in pressure was characterized and the minimum error of the difference between the simulation and test pressure values was

0.049, with a maximum value of 0.14. The average velocity value of the outlet at different angles of rotation was derived from the simulation, and both the simulation and test values for the wetted radius increased gradually with increase in the sprinkler rotation angle. The absolute error of the simulation and test ranged from 0.07 to 0.16. This shows that the turbulence model for simulation provides accurate results for the new variable-rate fluidic sprinkler. The mainstream region and the variable velocity regions were clearly distinguished. According to the flow fields, structural optimization schemes for the channels can improve the performance of the sprinkler.

ACKNOWLEDGEMENTS

The authors gratefully acknowledge that the work presented in this paper has been supported by the National Natural Science Foundation of China No. 51109098, the China National High-Tech (863) Program Grant No. 2011AA100506, and the National Agricultural Technology Transformation Program No. 2011GB2C100015.

REFERENCES

1. Ahmadi, M. M., Ayyoubazdeh, S. A., Montazeri Namin, M. and Samani, M.V. A 2D Numerical Depth-averaged Model for

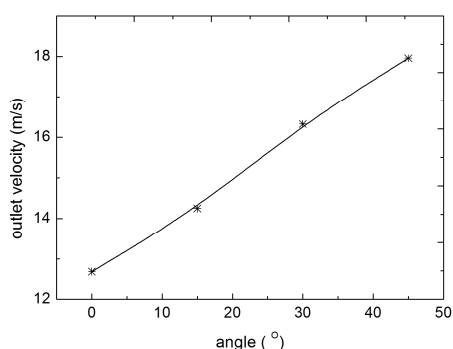


Figure 17. The changed curve of the outlet velocity at different angles.

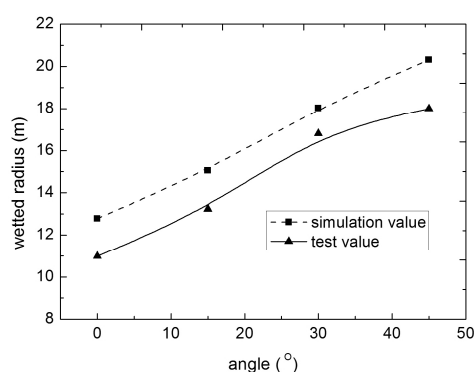


Figure 18. Comparison of the relationship between the angle and wetted radius obtained by simulation and experiment.



- Unsteady Flow in Open Channel Bends. 2009. *J. Agr. Sci. Tech.*, **11**: 457-468.
2. John D., Anderson J. R. 2004. *Computational Fluid Dynamics: The Basics with Applications*. Tsinghua University Press, Beijing, China.
 3. ASABE Standards. R2007. S398.1: Procedure for Sprinkler Testing and Performance Reporting. ASABE, St. Joseph, Mich.
 4. ASABE Standards. R2007. S436.1: Test Procedure for Determining the Uniformity of Water Distribution of Center Pivot and Lateral Move Irrigation Machines Equipped with Spray or Sprinkler Nozzles. ASABE, St. Joseph, Mich.
 5. Christiansen, J. E. 1942. Irrigation by Sprinkling. *California Agricultural Experiment Station Bulletin 670*, University of California, Berkeley, California.
 6. Fraisse, C. W., Duke, H. R. and Heermann, D. F. 1995. Laboratory Evaluation of Variable Water Application with Pulse Irrigation. *Trans. ASAE*, **38(5)**: 1363-1369.
 7. Hendawi, M., Molle, B., Folton, C. and Granier, J. 2005. Measurement Accuracy Analysis of Sprinkler Irrigation Rainfall in Relation to Collector Shape. *J. Irrig. Drain. Eng.*, **131(5)**: 477-483.
 8. Keller, J. and Bliesner, R. D. 1990. *Sprinkler and Trickle Irrigation*. Van Nostrand Reinhold, New York, NY, 652 PP.
 9. Li, H., Yuan, S. Q., Xiang, Q. J., Wang, C. 2010. Theoretical and Experimental Study on Water Offset Flow in Fluidic Component of Fluidic Sprinklers. *J. Irrig. Drain. Eng.*, **137(4)**: 234-243.
 10. Li, H., Xie, F. Q., Lang, T., Tang, Y., Jin, S. D. 2004. Research Status in Quo and Development Trend in Full-jet-flow Sprinkler Head. *China Rural Water Hydropower*, **(3)**: 90-92.
 11. Li, J., Li, Y., Kawano, H. and Yoder, R. E. 1995. Effects of Double-rectangular-slot Design on Impact Sprinkler Nozzle. *Trans. ASAE*, **38(5)**: 1435-1441.
 12. Perry, C. D., Dukes, M. D. and Harrison, K. A. 2004. Effects of Variable-rate Sprinkler Cycling on Irrigation Uniformity. *ASAE Annual International Meeting*, Ottawa, Canada. PP. 879-889.
 13. Sourell, H., Faci, J. M. and Playán, E. 2003. Performance of Rotating Spray Plate Sprinklers in Indoor Experiments. *J. Irrig. Drain. Eng.*, **129(5)**: 376-380.
 14. Tuo, Y. F., Yang, L. H., Chai, C. L., Gao, H. Y. 2006. Experimental Study and Theoretical Formula of the Sprinkler Wetted Radius. *Trans. CSAE*, **22(1)**: 23-26.
 15. Tso, T. C. 2004. Agriculture of the Future. *Nature*, **428**: 215-217.
 16. Van Doormal, J. P. and Raithby, G. G. 1984. Enhancement of the SIMPLE Method for Predicting Incompressible Fluid Flows. *Numer Heat Transf*, **7**: 147-163.
 17. Wang, F. J. and Wang, W. E. 2006. Research Progress in Analysis of Flow Passage in Irrigation Emitters Using Computational Fluid Dynamics Techniques. *Trans. CSAE*, **22(7)**: 118-122.
 18. Yan, H. J. and Jin, H. Z. 2004. Study on the Discharge Coefficient of Non-rottable Sprays for Center-Pivot System. *J. Irrig. Drain.*, **23(2)**: 55-58.
 19. Yan, H. J., Ou, Y. J., Kazuhiro Nakano, Xu, C. B. 2009. Numerical and Experimental Investigations on Internal Flow Characteristic in the Impact Sprinkler. *Irrig. Drain. Sys.*, **23**: 11-23.
 20. Yan, H. J., Liu, Z. Q., Wang, F. X., Yang, X. G., Wang, M. 2007. Research and Development of Impact Sprinkler in China. *J. China Agricultural University*, **12(1)**: 77-80.
 21. Yuan, S. Q., Zhu, X. Y., Li, H., Ren, Z. Y. 2005. Numerical Simulation of Inner Flow for Complete Fluidic Sprinkler Using Computational Fluid Dynamics. *Trans. CSAM*, **36(10)**: 46-49.

شبیه سازی عددی و مطالعه آزمایشی نوع جدیدی از آبپاشهای سیالی (Fluidic) با دبی متغییر

ج. پ. لیو، س. ک. یوان، ه. لی، و ژ. ی. ژو

چکیده

به لحاظ پیچیدگی ساختار دستگاه تنظیم فشار که در بیشتر آبپاشها برای آبیاری متغییر به کار می رود، مشاهده رفتار جریان آبی که از میدان جریان گذر میکند مقدور نیست. در این مقاله، یک مدل عددی یکپارچه و سه بعدی که مبتنی بر ویژگی های ساختاری آبپاشهای سیالی برپا شده بود برای شبیه سازی توزیع میدان جریان با استفاده از دینامیک سیالات محاسباتی (CFD) به کار رفت. در ادامه کار، یک نوع جدید آبپاش سیال (BPXH) مورد مطالعه قرار گرفت و ناحیه اصلی جریان و ناحیه با سرعت متغییر به وضوح از هم تمیز داده شد و جزئیات تغییرات فشار مورد بحث قرار گرفت. نتایج حاکی از آن است که روش شبیه سازی مزبور داده های کافی برای تجزیه و تحلیل تغییرات فشار آبپاش و سرعت خروج را فراهم میکند. کمترین اشتباه بین مقدار فشار به دست آمده از مدل شبیه سازی و داده های اندازه گیری برابر 0/49 و حداکثر آن 0/140 بود. یافته های مطالعه نشان میدهد که مدل آشوبی می تواند رابطه میان سرعت خروجی و شعاع خیس شده را به خوبی پیش بینی کند. سرعت خروج در طی فرایند شبیه سازی و تحت شرایط مرزی متغییر ورودی آبپاش بین ۱۲/۶ تا ۱۷/۹ متر در ثانیه متغییر بود. نیز، شعاع خیس شده شبیه سازی شده و اندازه گیری شده هر دو به تدریج با افزایش زاویه چرخش آبپاش بیشتر شدند. مقدار اشتباه مطلق در شبیه سازی و اندازه گیری آزمایشی بین 0/07 و 0/16 بود. به این قرار، در طراحی دستگاه تنظیم فشار برای نوع جدیدی از آبپاشهای سیالی با دبی متغییر، کار برد اصول دینامیک سیالات محاسباتی وسیله خوبی است.